Geophys. J. Int. (1991) **105,** 513–527

Analytical models of the effective permeability of sand–shale reservoirs

J. F. McCarthy

Applied Mechanics and Electromagnetics Group, BHP Melbourne Research Laboratories, PO Box 264, Clayton, Victoria 3168, Australia

Accepted 1990 December 20; Received 1990 December 6; in original form 1990 July 10

SUMMARY

A study is made of the dependence of the effective permeability of sand–shale reservoirs on the geometry of the shale inclusions. Numerical simulations are described in which factors such as the orientation and the degree of anisotropy of the shales, their volume fraction and the permeability contrast ratio between the shale and the sandstone were varied. Two different reservoir models were used in the simulations: one in which the shales were in the form of random, overlapping spheroidal inclusions, and one in which the shales were generated by a geostatistical technique. The computed effective permeability data are compared with a variety of analytical models in an attempt to discover 'rules of thumb' for the estimation of the effective permeability of sand–shale reservoirs for use in a range of practical situations. The main technical way in which this study advances on previous work is in its use of a computationally efficient, random walk algorithm for calculating the effective permeability, which has enabled larger volumes to be simulated and, hence, a thorough investigation of finite-size effects to be made. Another advantage of the work reported here is the general nature of the sand–shale geometries used in the numerical simulations and the extensive comparisons with analytical models.

Key words: effective permeability, heterogeneity, random walks, sand–shale reservoirs.

1 INTRODUCTION

Simulators used to study fluid flow in reservoirs are generally based on a finite-difference scheme. The user must provide input for the simulator in the form of a parametrized model of the reservoir. This involves making a suitable decomposition of the reservoir volume into gridblocks and assigning gridblock values for the reservoir parameters (e.g. absolute and relative permeabilities and porosities). It is implicitly assumed that the reservoir rock properties are homogeneous on the scale of the gridblocks used; whereas, in fact, it is known that reservoirs contain heterogeneities on all scales and that it is impossible in practical simulations to use a grid which is fine enough to resolve all their effects. Hence, it becomes necessary to estimate 'effective' gridblock values for reservoir parameters.

It is problematic to estimate effective values for transport properties, such as permeability, because the correct values depend on unknown factors such as the orientation of heterogeneities with respect to the direction of fluid flow. Taking an arithmetic mean of the constituent permeability values in a sample volume is generally inadequate. The arithmetic mean gives the correct measure of the effective permeability in the case when the sample volume is layered and the direction of flow is parallel to the layers. However, when the direction of flow is perpendicular to the layers, the effective permeability is given by the harmonic mean. In general, the value of the effective permeability lies somewhere between these two extremes and it is often approximated by the geometric mean of the constituent permeabilities. [Note: perturbation theory has shown the geometric mean approximation to be valid in the case when the variance of the permeability distribution is small. See e.g. King (1987) and Drummond & Horgan (1987)].

It is important to consider how heterogeneity on different scales affects the results of reservoir simulations. Small-scale heterogeneity (i.e. variability due to the transition from one rock-type to another and to factors such as grain-size, 'muddiness' and carbonation) can be accounted for by means of a straight-forward averaging procedure, while large-scale heterogeneity (i.e. variability due to the geological layers deposited by the sedimentary process) can be dealt with by including extra layers in the simulation. It is heterogeneities on intermediate scales which cause the most problems. A common cause of intermediate-scale heteroge-

neity is the presence of low-permeability barriers or 'discontinuous' shale inclusions. ('Discontinuous' in the sense of being uncorrelatable between wells. The term 'stochastic' is often used.) Thus; considerable research effort has been directed towards calculating the effective permeability of sandstone reservoirs with discontinuous shale inclusions. In simulations of 'sand–shale' reservoirs it is usual to make a rough division of the reservoir into homogeneous regions of high and low permeability. Of course, in real reservoirs, the sandstone and shale phases themselves consist of rocks of varying permeability, but the permeability variations within each phase are not nearly as important as the contrast between phases, which may be as much as five to seven orders of magnitude. Numerical work by Desbarats (1987a and b) supports the validity of the bimodal approximation for the permeability distribution. The use of the bimodal approximation allows us to apply results from the theory of two-component composite materials.

Two recent publications demonstrate the advantages of including a sophisticated approach to the treatment of discontinuous shales in reservoir simulations as follows.

(i) Begg, Carter & Dranfield (1989) were able to assign appropriate values for the effective permeability parameters to simulator gridblocks in simulations of the Sherwood Reservoir in Dorset, UK, which is a heterogeneous sandstone reservoir. As a result, a good match between the simulator predictions and observed production data was achieved with minimal fine tuning of the model parameters.

(ii) In another British Petroleum project, Haldorsen (1989) was able to improve predictions of the production rates of oil, water and gas flowing from a single well in a North Sea Reservoir. The reservoir contained a thin oil column sandwiched between a gas cap and an active acquifer. In this project, the accurate description of discontinuous shales around the well was very important for an understanding of the gas/water coning mechanism.

The particular problem which is addressed in this paper is the dependence of the effective permeability of sand–shale reservoirs on the geometry of the shale inclusions. Numerical simulations were carried out, varying such factors as the orientation and the degree of anisotropy of the shales, their volume fraction and the permeability contrast ratio between the shale and the sandstone. Two different reservoir models were used: one in which the shales were in the form of random, overlapping spheroidal inclusions, as has previously been considered by several researchers including Deutsch (1989), and one in which the shales were generated by a geostatistical technique, following the approach of Desbarats (1987a). The numerical data are displayed in the form of graphs of effective permeability versus shale volume fraction. The numerical effective permeability curves are compared with a variety of analytical models in an attempt to discover 'rules of thumb' for the estimation of the effective permeability of sand–shale reservoirs for use in a range of practical situations.

The analytical models which have been considered are described in detail in Section 2. They fall into two major categories:

(i) dilute suspensions, bounds and effective medium theories; and

(ii) generalized percolation models.

Approach (i) gives explicit formulae which depend only on the volume fraction and the anisotropy ratio of the shale inclusions, while (ii) provides a model with one or two parameters which must be fitted to the numerical data. The results of this paper show that dilute suspensions, bounds and effective medium theories are relevant and that their predictions are quantitatively useful in some cases. However, they cannot provide an acceptable estimate of the effective permeability for all possible geometries consistent with a given shale volume fraction and anisotropy ratio. On the other hand, the generalized percolation model approach leads to an easily applicable method for estimating the effective permeability. For a given anisotropy ratio, a range of parameters for the model can be specified which include the results for a range of sand–shale geometries. This determines empirical bounds for the effective permeability curve which can be narrowed down by making inferences about factors such as the degree of alignment of the shale inclusions.

A great deal of research has already been done on the problem of calculating the effective permeability of sand–shale reservoirs, notably by Begg *et al.* (Begg & King 1985; Begg, Chang & Haldorsen 1985), Desbarats (1987a and b) and Deutsch (1989). The main technical way in which this paper advances on previous work is in its use of a computationally efficient, random walk algorithm (McCarthy 1990a and b) for calculating the effective permeability, which has enabled larger volumes to be simulated and, hence, a thorough investigation of finite-size effects to be made. Random walk algorithms are commonly used in studies of diffusion and percolation theory (e.g. Haus & Kehr 1987; Havlin & Ben-Avraham 1989) and in calculating effective conductivities of composite materials (e.g. Schwartz & Banavar 1989). They are discussed in detail in Section 3. Another advantage of the work reported here is the general nature of the sand–shale geometries used in numerical simulations. A wealth of numerical data have been generated and compared with what is, to the best of the author's knowledge, a comprehensive list of relevant analytical models. Thus; it is intended that this paper should provide both a review and an extension of previous work. (Note added in proof: of course, it is too ambitious to suggest that the analytical models considered in this paper constitute a 'comprehensive' list and the author is indebted to the referee for drawing attention to the work of R. M. Christensen, 1990, *J. Mech. Phys. Solids*, **38,** on the elasticity problem.)

The arrangement of this paper is as follows. In Section 2, a discussion of analytical models is given. In Section 3, numerical methods are discussed. Section 4 contains a description of simulations and results and Section 5 contains conclusions and general discussion.

2 ANALYTICAL MODELS

The analytical models discussed fall into two main categories:

(i) dilute suspensions, bounds and effective medium theories; and

(ii) generalized percolation models.

To understand what follows it should be noted that the effective permeability, K^*, of a material is defined by Darcy's Law, which gives the relationship between the average fluid flow rate, $\overline{q}$, and the average piezometric head, $\overline{\nabla\Phi}$, across a cross-section of the material, i.e.

$$\overline{q} = K^* \overline{\nabla\Phi}. \tag{2.1}$$

Effective permeability is one example of a 'transport coefficient'. Other transport coefficients include electrical conductivity, dielectric constant and thermal conductivity. These transport coefficients are defined in relation to the flow of other physical quantities, such as electrical charge and heat. The mathematical equations which describe the flow of these quantities are equivalent to the fluid flow equations (2.1). Thus; the literature relating to electrical and thermal conduction is directly applicable to the effective permeability problem. In the following, results will often be given in terms of the effective conductivity of material composites since this is the area in which most of the relevant theoretical work has been done.

2.1 Dilute suspensions, bounds and effective-medium theories

The effective conductivity of two-component composites is determined by the conductivities of the constituent phases, their volume fractions and the composite geometry. Exact relations are available for very dilute suspensions of randomly oriented inclusions in a continuous matrix (see the excellent review by Batchelor 1974). For example, the effective conductivity, ϵ^*, of a dilute suspension of spheres (conductivity ϵ_1, volume fraction f_1) in a continuous matrix (conductivity ϵ_2, volume fraction f_2) is given by:

$$\epsilon^* = \epsilon^2 + \frac{3f_1\epsilon_2(\epsilon_1 - \epsilon_2)}{2\epsilon_2 + \epsilon_1}. \tag{2.2}$$

This relation was first derived by Maxwell (1873). Polder and Van Santen (1946) generalized the expression to give the effective conductivity of a dilute suspension of ellipsoids with a random distribution of orientations:

$$\epsilon^* = \epsilon_2 + \frac{f_1(\epsilon_1 - \epsilon_2)}{3} \sum_{i=1,2,3} \frac{\epsilon_2}{[\epsilon_2 + A_i(\epsilon_1 - \epsilon_2)]}, \tag{2.3}$$

where A_i are the depolarizing factors along the ellipsoid axes 1, 2 and 3.

Strictly speaking, dilute suspension relations are only valid in the case in which the inclusions are so far apart that the field lines near one inclusion are approximately the same as though that inclusion were alone in an infinite matrix. The volume fraction at which one can no longer consider the inclusions to be non-interacting depends on their shape. For spheres, experiments indicate that corrections to the dilute approximation must be made for volume fractions over about 0.05 and the condition will be even more restrictive for general ellipsoids (Sen & Torquato 1989).

Begg & King (1985) used the dilute suspension method to derive a simple, approximate expression for the effective vertical permeability, K^*, of a sandstone reservoir containing aligned rectangular shale inclusions:

$$K^* = \frac{K_{ss}(1 - f_{sh})}{(1 + SD/3)^2}, \tag{2.4}$$

where K_{ss} is the sandstone permeability, f_{sh} is the volume fraction of shale, S is the number of shales per metre, and D is the mean shale length. Expression (2.4) only holds for impermeable shales and for small shale volume fractions.

The dilute suspension method can be improved by taking a self-consistent, or 'effective medium', approach in which one considers the inclusion to be surrounded by a homogeneous medium of conductivity ϵ^* (e.g. Hale 1976). The effective-medium relation for spheres is

$$\frac{f_1(\epsilon^* - \epsilon_1)}{\epsilon_1 + 2\epsilon^*} + \frac{f_2(\epsilon^* - \epsilon_2)}{\epsilon_2 + 2\epsilon^*} = 0. \tag{2.5}$$

This relation is symmetric in components 1 and 2. It has been derived in a variety of contexts as an approximation for the effective transport properties of random, uncorrelated two-component mixtures (in which the two phases are symmetric but have no particular geometry). Thus; it was derived by Bottcher (1945), in the context of dielectrics, by Kirkpatrick (1973), in the context of effective conductivities of random resistor networks above the percolation threshold, and by Dagan (1979), in the context of effective permeabilities. Desbarats (1987a) showed that equation (2.5) is a good approximation for the effective permeability of sand–shale reservoirs calculated in numerical simulations at low shale volume fractions when the permeability of each grid block is assigned at random to be either $K_{sh}(\approx 0)$ or $K_{ss}(=1)$.

More sophisticated, generalized self-consistent schemes can be developed. For example, one can consider a sphere of conductivity ● coated by a material of conductivity ϵ_2 in the proportion determined by the specified volume fraction, and all surrounded by a homogeneous medium of conductivity ϵ^*. The effective conductivity relation derived using this scheme becomes exact for the case of the 'composite spheres assemblage', which is a material completely filled by coated spheres of different sizes. This relation is (e.g. Hale 1976)

$$\epsilon^* = \epsilon_2 + \frac{f_1}{[1/(\epsilon_1 - \epsilon_2)] + (f_2/3\epsilon_2)}. \tag{2.6}$$

This relation is asymmetric in components 1 and 2, as a consequence of the fact that one of the components is completely surrounded by the other.

Willis (1977) derived effective-medium relations for the transport properties of bodies containing aligned ellipsoidal inclusions. His work was explicated upon by Bergman (1982) in studies of a composite of coated ellipsoids, analogous to the composite spheres assemblage described above. In this paper we will use Bergman's notation and give the results of his generalized self-consistent analysis. These results are used in comparisons with numerical data in Section 4.

Consider a composite of coated ellipsoids, of different sizes but with a constant aspect ratio. The surfaces of the inclusions are given in ellipsoidal coordinates by $\xi = \text{const}$, where the 3-D ellipsoidal coordinates ξ, η, ζ are defined by

$$x = \pm\left(\frac{(\xi + a^2)(\eta + a^2)(\zeta + a^2)}{(b^2 - a^2)(c^2 - a^2)}\right)^{1/2},$$

$$y = \pm\left(\frac{(\xi + b^2)(\eta + b^2)(\zeta + b^2)}{(c^2 - b^2)(a^2 - b^2)}\right)^{1/2},$$

$$z = \pm\left(\frac{(\xi + c^2)(\eta + c^2)(\zeta + c^2)}{(a^2 - c^2)(b^2 - c^2)}\right)^{1/2}.$$

These functions are the three solutions of the following cubic equation for u:

$$\frac{x^2}{a^2+u}+\frac{y^2}{b^2+u}+\frac{z^2}{c^2+u}=1, \tag{2.7}$$

and they satisfy

$$\xi \geq \eta \geq \zeta.$$

The effective conductivity, ϵ^*, of the above composite is exactly the same as that which is derived using the generalized self-consistent method for an ellipsoidal core, surface $\xi = \xi_1$, of conductivity ϵ_1 coated by an ellipsoidal shell, surface $\xi = \xi_2$, of conductivity ϵ_2 and embedded in a homogeneous medium of conductivity ϵ^*. The self-consistent relation is shown by Bergman to be

$$\frac{\epsilon_2-\epsilon^*}{\epsilon_2}=\frac{f_1}{\epsilon_2/(\epsilon_2-\epsilon_1)-L(\xi_1)+f_1L(\xi_2)}, \tag{2.8}$$

where f_1 is the volume fraction of the ϵ_1 core, and $L(\xi_1)$ and $L(\xi_2)$ are the depolarization factors of the core surface, $\xi = \xi_1$, and the outer shell surface, $\xi = \xi_2$, respectively.

Our objective is to obtain an estimate for the effective vertical permeability of sandstone reservoirs with aligned spheroidal shale inclusions, to be compared with data from numerical simulations. For this purpose we need to consider the case of oblate spheroidal surfaces whose symmetry axis points along the x axis, i.e. $b = c > a$. The depolarization factor is then given by

$$L(E)=\left(1+\frac{1}{E^2}\right)\left(1-\frac{1}{E}\arctan E\right), \tag{2.9}$$

where

$$E(\xi_1)=\sqrt{e_1^2-1} \tag{2.10}$$

and $e_1 (= e \geq 1)$ is what we define as the anisotropy ratio of the spheroid, i.e. the ratio of the longer to the shorter semi-axis. E_2 is determined from the relationship between the volumes of the spheroidal core and its shell:

$$f_1=\frac{(1-E_1^2)/E_1^3}{(1-E_2^2)/E_2^3}. \tag{2.11}$$

So, given the anisotropy ratio e of the spheroidal core, E_1, L_1, E_2 and L_2 can be found using equations (2.9)–(2.11). Then the self-consistent relation, equation (2.8), can be solved to find ϵ^* as a function of e and f_1.

The limiting case of aligned penny-shaped cracks, obtained by letting $e \to \infty$ and $\epsilon_1 \to 0$, will be useful when considering highly anisotropic inclusions. The self-consistent relation for ϵ^* then reduces to (Benveniste & Miloh 1989):

$$(1-f_1)^{1/2}\left(\frac{1}{\epsilon^*}\right)-\frac{2f_1}{e\pi}\left(\frac{1}{\epsilon^*}\right)^{1/2}-(1-f_1)^{1/2}=0. \tag{2.12}$$

Fig. 1 shows a comparison between the effective permeability curves derived using the relation for oblate spheroids, equation (2.8), and the (simpler) crack approximation, equation (2.12), for a value of the anisotropy ratio of $e = 5$. The curves lie very close together at this value of e and it can be shown that they converge as $e \to \infty$.

In order to find an estimate for the effective horizontal permeability, we need to consider prolate spheroidal surfaces whose symmetry axis points along the x axis, i.e. $b = c < a$. The depolarization factor is then given by

$$L(E)=\frac{1-E^2}{2E^3}\left(\ln\frac{1+E}{1-E}-2E\right), \tag{2.13}$$

where now

$$E(\xi_1)=\sqrt{1-\frac{1}{e_1^2}} \tag{2.14}$$

and E_2 is determined from the relation

$$f_1=\frac{(1-E_1^2)/E_1^3}{(1-E_2^2)/E_2^3}. \tag{2.15}$$

As before, E_1, E_2, L_1 and L_2 can be found and the self-consistent relation, equation (2.8), solved to find ϵ^* as a function of e and f_1.

For prolate spheroids, the limiting case obtained by letting $e \to \infty$ corresponds to the case of aligned cylinders. The effective conductivity for current flow along the axis of the cylinders then reduces to the arithmetic mean:

$$\epsilon^* \approx f_1\epsilon_1 + f_2\epsilon_2.$$

In practice, we found that the effective horizontal permeability obtained in numerical simulations could be well-approximated by the arithmetic mean for large anisotropy ratios.

Complementary to the approximations obtained using the effective-medium approach are the rigorous upper and lower bounds on the effective conductivity of two-component composites derived by a variety of mathematical techniques including variational methods (e.g. Hashin & Shtrikman 1962) and continued fractions (Milton 1987). Bounds become progressively closer together as more information about the structure of the material is included (usually, in the form of n-point correlation functions). If all that one knows about the material is the volume fractions of its constituents, then the most restrictive bounds which one can

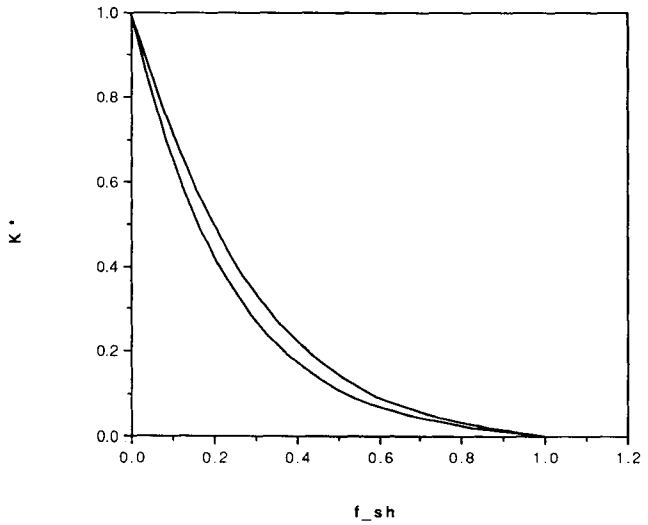

Figure 1. Effective permeability curves derived using the generalized self-consistent relation for oblate spheroids [lower curve, see equation (2.8) in the text] and the crack approximation [upper curve, see equation (2.12) in the text] for a value of the anisotropy ratio of $e = 5$.

stipulate are the Wiener bounds (Wiener 1912):

$$(f_1\epsilon_1^{-1} + f_2\epsilon_2^{-1})^{-1} \leq \epsilon^* \leq f_1\epsilon_1 + f_2\epsilon_2. \quad (2.16)$$

This is the well-known result that the effective conductivity of a material is bounded by the arithmetic and harmonic means of the conductivities of its constituents. The Wiener bounds are achieved for layered materials: the upper bound (arithmetic mean) when current flows along the layers and the lower bound (harmonic mean) when current flows perpendicular to the layers (*cf.* resistors in parallel and in series). They are not very restrictive in the case of interest when $\epsilon_1 \ll \epsilon_2$.

Most of the mathematical derivations of higher order bounds (and their associated effective-medium relations) include the assumption of statistical isotropy. It is only recently that techniques have been developed for the more complicated case of macroscopically anisotropic composites (e.g. oriented ellipsoidal inclusions and layered media). Notable are the work of Milton & Kohn (1988) and Sen & Torquato (1989). Their work provides us with rigorous nth-order bounds for the effective conductivity of statistically anisotropic materials in terms of integrals over n-point correlation functions. The practical implementation of these bounds is limited by the degree of statistical information which can actually be determined for a particular material. In the case of sand–shale reservoirs, it would be unrealistic to expect to obtain information about correlation functions greater than second order. In that case the bounds derived by Sen & Torquato (1989) reduce to those derived by Willis (1977) in his work on the transport properties of bodies with aligned ellipsoidal inclusions, for which we have already discussed the associated effective-medium relations.

2.2 Generalized percolation models

In numerical simulations of the effective permeability of sand–shale reservoirs, the sand–shale sequence is generally modelled by a 3-D grid with each gridblock being either sandstone or shale. If the shale is taken to have zero permeability then such a model is exactly of the kind treated by percolation theory. In percolation theory, questions are asked about the nature of the clusters of sandstone blocks which form as the volume fraction of sandstone is increased. In particular, if the permeability of the blocks is assigned randomly, then there is a critical volume fraction called the 'percolation threshold' at which a connecting cluster of sandstone blocks is first found across the medium, allowing percolation of fluid through the medium. The percolation threshold is known very accurately for cubic grids. It occurs at a critical shale volume fraction of

$$f_c(\text{cubic}) = 0.6883 \pm 0.0005. \quad (2.17)$$

For shale volume fractions above f_c the effective permeability is zero, while below the threshold it rises in a way which can be predicted from symmetric effective medium theory:

$$K^* = K_{ss}\left(1 - \frac{f_{sh}}{f_c}\right)^{1/m}, \quad (2.18)$$

where m is an exponent.

Unfortunately, percolation theory is not as relevant to calculating the effective permeability of sand–shale reservoirs as it might appear at first sight. Very little theoretical work has been done for the case when there are correlations between blocks or the material is not isotropic. [The exception is that some theoretical results have been obtained for Ising-correlated systems, e.g. Coniglio (1975), Evans (1987), and Kikuchi (1970).] There has been numerical work done on correlated percolation, notably the work of Pike & Seager (1974) on percolating systems of spheres, rods and other shapes. However, for the sand–shale reservoir problem, the only conclusions which can be drawn from such work are very general ones, such as that the introduction of correlations tends to increase the effective permeability [*cf.* the conclusion which was reached by Desbarats (1987a): 'Greater statistical continuity between adjacent grid block permeabilities enhances the ability of flow to bypass low permeability zones'].

Nevertheless, percolation theory can be useful in a generalized form, if we treat the percolation equation, equation (2.18), as an empirical model, rather than an anlytical relation. McLachlan (1987) proposed that equation (2.18) should hold for both isotropic and anisotropic inclusions, and for symmetric and asymmetric geometries, with appropriate values of the parameters m and f_c. Note that for $m = 1$ and $f_c = 2/3$ (corresponding to 'bond' percolation), equation (2.18) is equivalent to the symmetric self-consistent relation for spheres, equation (2.5), in the limiting case when $\epsilon_1 = 0$. Similarly, the asymmetric reltion, equation (2.6), in which one component is embedded in the other, can be expressed in the form of equation (2.18), correct to some order in a Taylor expansion, provided we take $\epsilon_1 = 0$, $f_c = 1$ and $m = 2/3$. Clearly, the relation derived by Begg & King (1985) equation (2.4), can be treated in the same way. Kirkpatrick (1973) developed an approximate result for the 'site' percolation problem which can be fitted by equation (2.18) with $m \approx 1.6$ and $f_c = 2/3$. Furthermore, McLachlan discusses how the self-consistent relations for randomly oriented and aligned spheroidal inclusions can be approximated by the generalized percolation model. For aligned spheroidal inclusions, he suggests that the parameters should be given by $f_c = 1$ and $m = (1 - L)$, where L is equivalent to the depolarization coefficient introduced before (see equations 2.9 and 2.13). He shows how the percolation model can be fitted to a variety of experimental data gathered from conductivity measurements on binary mixtures with both isotropic and anisotropic grain structures.

Let us consider how the generalized percolation model can be used to estimate the effective permeability of sand–shale reservoirs with a given geometry. It requires two parameters to be specified. The first corresponds to the critical volume fraction at which a medium with impermeable shale inclusions and with the same characteristic geometry would reach a percolation threshold. The second is an exponent, m, which depends on a characteristic coefficient (analogous to the depolarization coefficient) for the inclusions. This coefficient depends on the shape of the inclusions and whether they are oriented, partially oriented or random. For the reservoir models considered in this paper, m is not known. The approach that has been taken is to give a range of m values which provide empirical bounds

for all the numerical permeability data computed at a given anisotropy ratio.

In practice, reservoir rocks do not show percolation threshold behaviour. Thus; we can take $f_c = 1$. Then the generalized percolation model only requires one parameter to be specified. In that case it is equivalent to the power-averaging approach which was used by Journel, Deutsch & Desbarats (1986) and Deutsch (1989). Power-averaging involves modelling the effective permeability as a power average of the component permeabilities via the equation:

$$K^* = [f_{sh}K_{sh}^m + (1-f_{sh})K_{sh}^m]^{1/m} \tag{2.19}$$

where m is some averaging exponent. [Note: equation (2.19) includes the Wiener bounds as special cases: the upper bound when $m = 1$, and the lower bound when $m = -1$].

Equation (2.19) reduces to equation (2.18) when the shale inclusions are impermeable, i.e. $K_{sh} = 0$. It can also be used when the shale permeability if finite. In fact, the case of finite shale permeability was also discussed by McLachlan (1987) in a suggested extension to the generalized percolation model. He suggested that, provided $K_{sh} \ll K_{ss}$, one can use the empirical expression

$$\frac{f_{sh}(\Sigma_{sh} - \Sigma^*)}{\Sigma_{sh} + [f_c/(1-f_c)]\Sigma^*} + \frac{f_{ss}(\Sigma_{ss} - \Sigma^*)}{\Sigma_{ss} + [f_c/(1-f_c)]\Sigma^*} = 0$$

where $\Sigma_i = K_i^m$. However, we have not found this expression to be very useful in our work. The power-averaging model is simpler and just as comprehensive and, as discussed in the introduction, the assumption of impermeable shales is a good one when $K_{sh} \ll K_{ss}$.

3 NUMERICAL METHODS

In almost all previous numerical simulations, the effective permeability was calculated by first solving the flow equations using a finite-difference scheme, and then equating the integrated flux over any cross-section of the field with the flux corresponding to a field of uniform permeability, in accordance with Darcy's Law. Deutsch (1989) used the commercial flow simulator ECLIPSE for this purpose. The problem with using a finite-difference scheme is that it becomes very time-consuming for 'large' grid-sizes (i.e. for grid-sizes larger than about 30^3).

To the author's knowledge, the only previously suggested alternative to the finite-difference scheme for calculating effective permeabilities is a streamline method introduced by Begg & King (1985). This method is based on estimating the increase in streamline tortuosity due to the presence of shale inclusions. It involves tracing approximate streamlines through the grid. The algorithm fails for dense and/or complex shale configurations. It does not provide a controllable discretization of the flow equations in the same sense that the finite-difference method does, because it is not possible to rigorously analyse the way in which the streamline approximation introduces errors into the calculation.

Random walk algorithms provide a means of directly calculating the effective permeability of sand–shale reservoirs without explicitly solving the flow equations. They have a sound mathematical basis (e.g. Haus & Kehr 1987) and for large grids are much more efficient than finite-difference methods. (Note: the numerical work in this paper was done using grids of size 100^3 on an APOLLO work-station.) The constraints on the grid-size imposed by a given numerical method are a very important consideration in the calculation of effective permeability because it is the grid size that determines the range of scales of heterogeneity that can be solved. For example, if one wishes to simulate a medium which has an anisotropy ratio in the horizontal to vertical directions of 15:1 then a lattice of size at least 45^3 would be required to obtain statistically meaningful results (see Section 4.1 on finite-size effects). The effective permeability of a heterogeneous medium depends on the boundary conditions, which in turn depend on the volume being considered. The concept of effective permeability is only valid in the limit of the sampling volume being large with respect to the scale of the heterogeneities contained within it, in which case the condition of statistical homogeneity may be considered to apply. By using the random walk algorithm, it becomes possible to simulate shale inclusions of larger dimensions and larger anisotropy ratios than could previously have been considered.

Random walk algorithms, or more general diffusion algorithms, have proven to be useful in studies of effective conductivity (e.g. Schwartz & Banavar 1989). It is well-known that one can replace the conductivity problem with a diffusion problem using Einstein's relation which states that the diffusivity is proportional to the conductivity. Schwartz & Banavar (1989) used simulations based on Einstein's relation to provide a description of electrical transport in homogeneous disordered continuum systems. Until recently, this type of simulation had been restricted to two-component systems in which one of the components had zero conductivity, using an algorithm called the 'ant-in-a-labyrinth' algorithm (e.g. Stauffer 1985). McCarthy (1990a) described how to extend the simulations to the case in which both components had finite conductivity and, also, to the many-component conductivity case (McCarthy 1990b).

Let the sand–shale reservoir be modelled by a 3-D grid on which the blocks are designated to be either sandstone, of permeability K_{ss}, or impermeable shale. Then the 'ant-in-a-labyrinth' algorithm can be used to simulate an ensemble of random walks on the grid in the following way.

Imagine that the walks are performed by an army of ants. Initially, an ant is placed on a randomly chosen gridblock. At each step of the algorithm, the ant chooses one of its neighbouring gridblocks at random and either moves there, if the block is permeable, or stays put, if it is impermeable. In either case, the simulation time is incremented by one unit. Periodic boundary conditions are imposed. The mean-square distance travelled by the ants, $\langle R^2(t) \rangle$, is directly related to the simulation time, t, for large t, via

$$\langle R^2(t) \rangle = Dt, \tag{3.1}$$

where $\langle\ \rangle$ denotes an average taken over the ensemble. The constant of proportionality, D, is a measure of the diffusivity of the composite, from which the permeability is calculated using an analogy of Eintein's relation.

The algorithm used in the numerical simulations described in this paper includes the ant-in-a-labyrinth algorithm as a special case and extends it to cover the case in which the shale blocks have finite permeability, K_{sh}. The gridblock

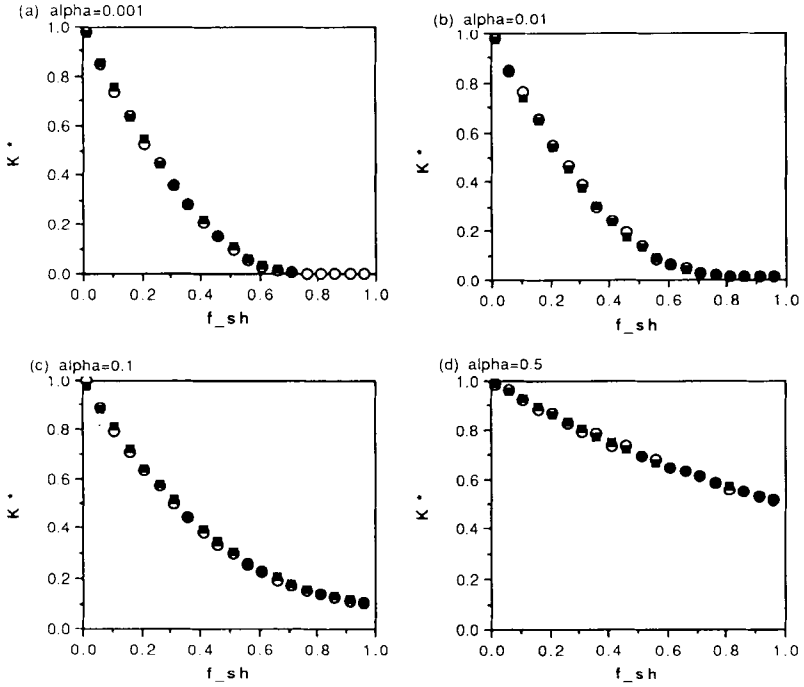

Figure 2. Effective permeability data computed in simulations of a random, uncorrelated, two-component system for four values of the permeability contrast ratio, $\alpha = K_{sh}/K_{ss}$: (a) $\alpha = 0.001$, (b) $\alpha = 0.01$, (c) $\alpha = 0.1$ and (d) $\alpha = 0.5$. Comparison between the random walk algorithm (circles) and the finite-difference method (squares).

permeabilities are scaled to that $K_{ss} = 1$ and $K_{sh} = K_{sh}/K_{ss}$. The ant at block i chooses one of its nearest neighbours, say j, at random and moves there with a probability given by

$$\Pi_{ij} = \frac{2K_iK_j}{K_i + K_j} \tag{3.2}$$

or stays put with probability $(1 - \Pi_{ij})$. In either case, the simulation time is incremented by one unit. Periodic boundary conditions are imposed.

Equation (3.2) defines the jump probability Π_{ij} to be given by the harmonic mean of the permeabilities of neighbouring blocks. This approximation ensures the conservation of mass flux across block boundaries but is by no means unique. It is analogous to the specification of transmissivity terms in the finite-difference method (see, e.g. Aziz & Settari 1979).

The validity of the random walk algorithm has been verified by comparisons with results obtained using the finite-difference method. Fig. 2 compares the values obtained for effective permeability versus shale volume fraction using the random walk algorithm and a finite-difference algorithm for four values of the permeability contrast ratio, $\alpha = K_{sh}/K_{ss}$, i.e. $\alpha = 0.001$, 0.01, 0.1 and 0.5. Averages were taken over 10 realizations of the permeability distribution on a 30^3 lattice, with 1000 ants taking 10 000 steps on each realization. The numerical results of the two algorithms are indistinguishable.

It is necessary to take averages over an ensemble of realisations of the permeability distribution because effective permeability is a statistical concept. Each realization must have the statistical characteristics of the medium and be large compared with the scale of the heterogeneities contained in it. In the figures shown in this paper error bars have been omitted for clarity but the reader may assume that the spread in the data shown in Fig. 3 is representative.

The random walk algorithm has some incidental advantages. For one thing, it is very easy to program. For another, the three (possibly different) values of the effective permeability in the three principle directions can be obtained in one simulation, rather than requiring separate simulations with the direction of flow changed, as is the case when using the finite-difference method. Fig. 4 shows the effective permeability results obtained in the x, y and z

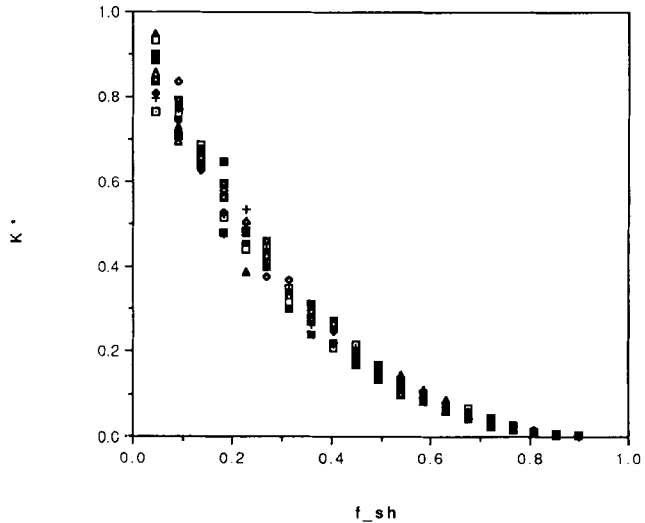

Figure 3. The spread in the effective permeability data computed over 10 realizations of the permeability distribution in simulations of the spheroidal reservoir model with spheroids of dimension $20 \times 20 \times 4$.

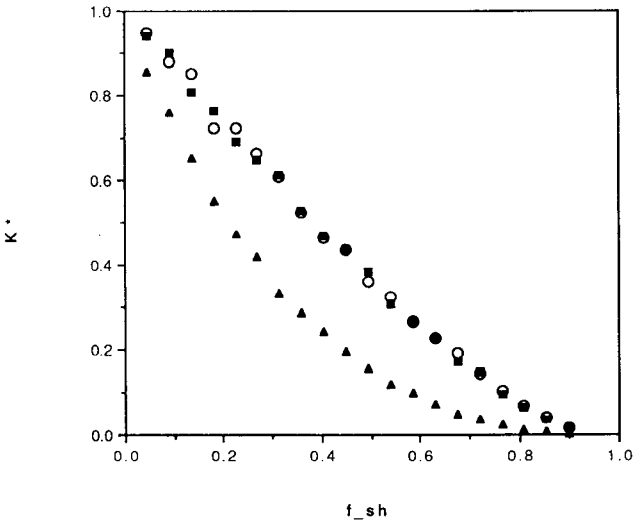

Figure 4. Effective permeability data computed in the x (circles), y (squares) and z (triangles) directions in a simulation of the spheroidal reservoir model with spheroids of dimensions $20 \times 20 \times 4$.

directions in one simulation of the spheroidal reservoir model with spheroids of dimensions $20 \times 20 \times 4$. As expected, the results for the effective permeability in the x and y directions (i.e. effective horizontal permeability) lie very close together because this particular reservoir model is isotropic in the x–y plane. In addition, they lie above the results for the z direction (i.e. effective vertical permeability), as expected. The random walk algorithm can be modified to deal with the case when local (block) permeability is not an isotropic scalar by giving different weights to the random walk in different directions.

4 RESULTS

4.1 Description of simulations

As mentioned in the introduction, simulations were performed for two different reservoir models—one in which the shales were in the form of randomly placed, overlapping spheroidal inclusions, and one in which the sand–shale geometry was generated by a geostatistical technique, following the approach of Desbarats (1987a). The

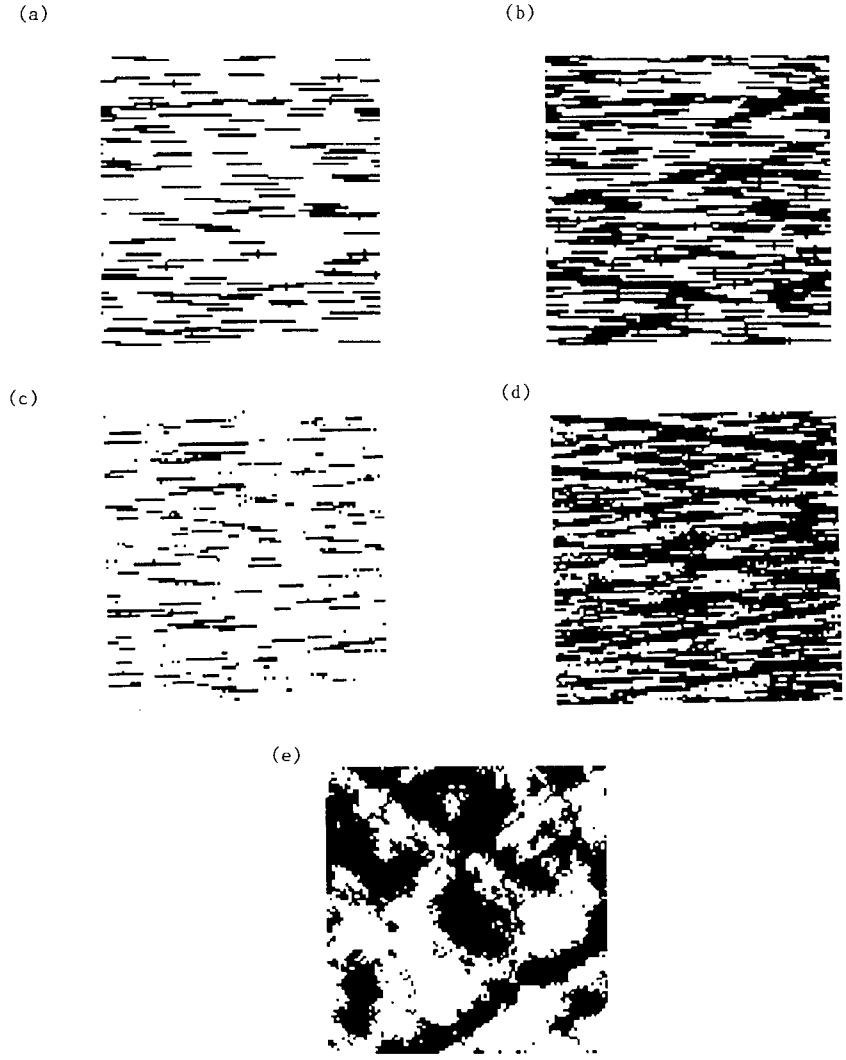

Figure 5. Cross-sections of the sand–shale permeability distributions generated for both the spheroidal and geostatistical models: (a) vertical cross-section, $f_{sh} = 0.2$, spheroidal model, (b) vertical cross-section, $f_{sh} = 0.5$, spheroidal model, (c) vertical cross-section, $f_{sh} = 0.2$, geostatistical model, (d) vertical cross-section, $f_{sh} = 0.5$, geostatistical model, and (e) horizontal cross-section, $f_{sh} = 0.5$, geostatistical model.

geostatistical simulations were quite realistic since they were designed to reproduce the first- and second-order statistics of the experimental sand–shale data gathered from an outcrop of the Assakao sandstone in the Tassili region of the Central Sahara [note: the Assakao data were first presented in Dupuy & Lefebvre du Prey (1968)]. The objective was to reproduce the arrangement of sands and shales with respect to one another, rather than simply modelling the observed geometry of individual shale lenses. Fig. 5 compares cross-sections of the sand–shale geometry generated for both the spheroidal and geostatistical models. As illustrated in Fig. 5(e), the simulations were isotropic in the horizontal $(x-y)$ plane. The vertical cross-sections look very similar. Allowing overlapping of the spheroidal inclusions seems to have the effect of introducing a range of shale lengths into the spheroidal model which mimic the output of the much more involved geostatistical model.

The simulation results are presented as graphs of effective permeability versus shale volume fraction. In the spheroidal case, a grid of size 100^3 was used. The effective permeability was calculated as an average over an ensemble of 10 realizations of the permeability distribution, with 10^3 random walkers on each realization and walks of length varying from 10^3 to 10^5 depending on the dimensions of the spheroids in the sample. In the geostatistical case, the grid-size used was 30^3 and averages were taken over an ensemble of five realizations.

Simulations were performed for different values of the permeability contrast ratio, $\alpha = K_{sh}/K_{ss}$. Detailed results are shown for $\alpha = 0.0001$ and $\alpha = 0.1$. Previous work (e.g. Desbarats 1987a) has shown that when $\alpha \leq 0.01$ the results obtained for the effective permeability are approximately the same as if the shale had been assumed to be impermeable (i.e. most of the flow occurs in the sandstone phase and the shale regions are bypassed). This is illustrated in Fig. 2 introduced previously.

The effect on the permeability of changing the orientation of the shale inclusions was studied by performing simulations in which a certain percentage of the inclusions in the spheroidal model were randomly oriented.

The horizontal to vertical anisotropy ratio used in the simulations was varied between 1:1 and 30:1. In the geostatistical case, since a grid of size 30^3 was used, the maximum anisotropy ratio which could be simulated and give statistically meaningful results was 10:1 (see Section 4.2 for an explanation of this).

4.2 Finite-size effects

In the simulations described, the fundamental length-scale in each direction i is given by the practical length, λ_i, over which scales are correlated. In the spheroidal reservoir model, λ_i is simply given by the ith dimension of the spheroidal inclusions. In the geostatistical simulations, λ_i is specified by explicitly giving the correlation function, $C(r_i)$, of the shale indicator random function. In our simulations, following the work of Desbarats (1987a), $C(r_i)$ is defined to be

$$C(r_i) = \exp\left[-\left(\frac{r_x^2}{\lambda_x^2}+\frac{r_y^2}{\lambda_y^2}+\frac{r_z^2}{\lambda_z^2}\right)^{1/2}\right]$$

where $\lambda_x = \lambda_y$ and $e = \lambda_x/\lambda_z$ is the anisotropy ratio.

When discussing finite size effects there are two factors to be considered:

(i) the size of λ_i relative to the corresponding linear dimension of the grid, L_i; and

(ii) the size of λ_i relative to the simulation step size, Δr. (Note: in the case of the random walk algorithm Δr_i is equivalent to the gridblock size.)

For an accurate calculation of effective permeability it is required that $\lambda_i \ll L_i$. The simulations of Desbarats (1987a), Deutsch (1989) and others (e.g. Smith & Freeze 1979) show that, in practice, the calculated effective permeability ceases to depend on the averaging volume when $\lambda_i < L_i/3$. The present work confirms this conclusion. Fig. 6 shows the results obtained in simulations of the aligned spheroidal reservoir model in which the spheroidal shale inclusions had dimensions $30 \times 30 \times 1$. The simulations were all performed on a 100^3 grid but the sample volume was effectively varied by varying the length of the random walks in accordance with equation (3.1). The different curves in Fig. 6 show the results obtained for walks of length $t = 10^2$, 10^3, 10^4 and 10^5. As can be seen, the results begin to converge for $t \geq 10^4$ which is equivalent to a sample volume of the order of 100^3. A similar analysis for shale inclusions of dimensions $15 \times 15 \times 1$ showed the results beginning to converge for $t \geq 10^3$. Our general procedure was to use walks of length $t = 10^3$ when the anisotropy ratio, e, was less than 15 and to use $t = 10^4$ for $e \geq 15$.

Consideration of factor (ii) mentioned above, leads to the stipulation that one should choose the gridblock size, Δr_i, such that $\Delta r_i < \lambda_i/3$. This is illustrated in Fig. 7 which compares the results obtained in simulations in which the anisotropy ratio was kept constant but the dimensions of the spheroidal inclusions were proportionately varied. Fig. 7(a) shows the results obtained for spheres of diameter $d = 1$, 2, 3, 5 and 10. Also shown are the analytical curves derived from Kirkpatrick's site percolation approximation (see Section 2.2) and asymmetric effective medium theory,

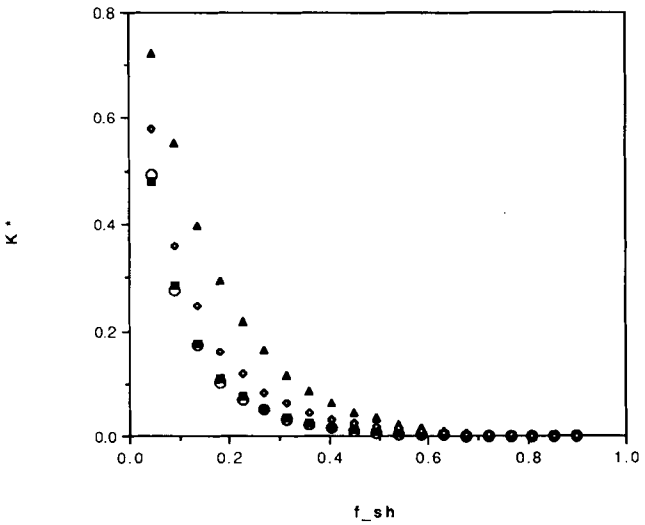

Figure 6. Effective permeability data computed in simulations of the spheroidal reservoir model with spheroids of dimensions $30 \times 30 \times 1$ using the random walk algorithm with walks of length $t = 10^2$ (triangles), $t = 10^3$ (diamonds), $t = 10^4$ (circles) and $t = 10^5$ (squares).

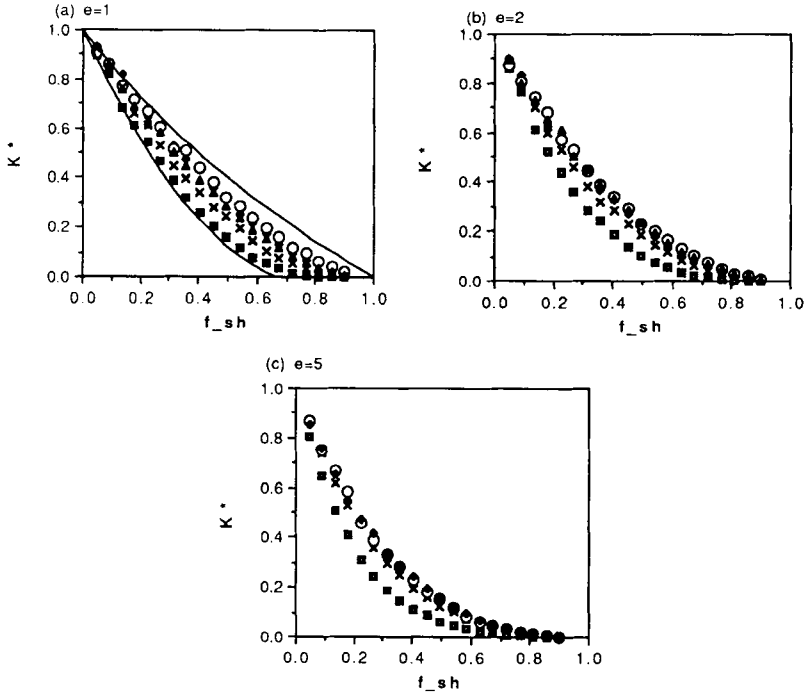

Figure 7. Effective permeability data computed in simulations in which the anisotropy ratio, e, was kept constant but the dimensions of the spheroidal inclusions were proportionately varied: (a) $e = 1:1$ (squares), $e = 2:2$ (crosses), $e = 3:3$ (triangles), $e = 5:5$ (diamonds) and $e = 10:10$ (circles), (b) $e = 2:1$ (squares), $e = 4:2$ (crosses), $e = 6:3$ (triangles), $e = 10:5$ (diamonds) and $e = 20:10$ (circles), and (c) $e = 5:1$ (squares), $e = 10:2$ (crosses), $e = 15:3$ (diamonds) and $e = 20:4$ (circles). (a) also shows the analytical curves derived from the site percolation approximation, Section 2.2 in the text, and from asymmetric effective medium theory, equation (2.6) in the text.

equation (2.6). In the case $d = 1$, a sphere is represented in our simulations by a single gridblock. Hence; this case is equivalent to the site percolation problem, in which a given fraction of gridblocks are randomly assigned to be shale. The computed results are well-fitted by Kirkpatrick's theory. As the diameter, d, of the spheres in the simulations is increased, the results show that the effective permeability also increases, as might have been expected from correlated percolation theory. The computed effective permeability curve approaches that derived from asymmetric effective medium theory, but always lies below it because we have allowed overlapping in our simulations. The curves begin to converge for $d > 3$. A similar observation can be made for the spheroidal results shown in Fig. 7(b), $e = 2$ and Fig. 7(c), $e = 5$.

The question of what the gridblock size should be relative to the correlation length seems to have been given less consideration in the literature than that of what the dimensions of the sample volume should be. However, it is equally important. In determining the gridblock size one is setting the minimum length-scale which can be resolved in the simulation. For example, by setting $\Delta r_i = \lambda_i$ one is stipulating that two non-overlapping shale inclusions will be at least a distance λ_i apart in the ith direction. In the case of spheres this corresponds to non-overlapping spheres being at least one diameter apart. Another way of looking at this case is to note that one is effectively setting the sandstone correlation length to be λ_i; thus making the geometry symmetric in the sandstone and shale phases whereas it is desired to simulate an asymmetric, inclusion-type geometry.

Many of the results quoted in this paper are for simulations in which the correlation length in the vertical (z) direction was set equal to the gridblock-size, in order to be able to study larger anisotropy ratios and for ease of comparison with published results of Desbarats (1987a) and Deutsch (1989). This is true of the geostatistical simulations and also of the simulations with spheroidal inclusions of dimensions $N \times N \times 1$. Of course, these are perfectly valid geometries and comparisons can be made between the computed results to derive qualitative conclusions about questions such as the effect of varying the anisotropy ratio. However, one should not imagine that the results are quantitively correct for a generic sand–shale geometry of anisotropy ratio $e = N$. For that, a complete study of the finite-size effects would have to be carried out (*cf.* Fig. 7 for spheroidal shale inclusions of dimensions $kN \times kN \times k$).

4.3 Results for $K_{sh}/K_{ss} \equiv \alpha = 0.0001$ (≈ 0)

Figure 8 shows the effective permeability results computed in simulations of the spheroidal reservoir model with spheroids of anisotropy ratio $e = 1:1$, $2:1$, $5:1$, $10:1$, $15:1$ and $30:1$, respectively. Also included in the figure are the analytical curves obtained from the generalized self-consistent relations for a composite of aligned oblate spheroids (see equation 2.8). For $e = 10$, the analytical curve provides an excellent fit to the simulation data. For $e > 10$ the curves have the correct shape but lie below the data points, while for $e < 10$ the curves lie above the data points. These results are qualitatively explained by considering the following two competing effects to do with overlapping.

(i) The percolation effect, which is absent in the host-inclusion geometry assumed in the derivation of the

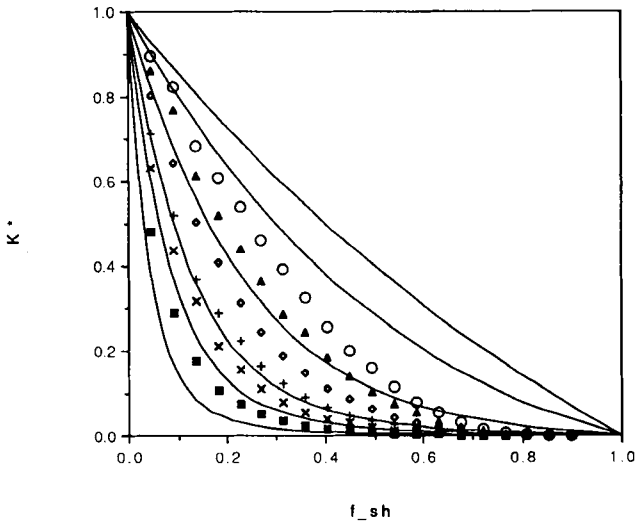

Figure 8. Effective permeability data computed in simulations of the spheroidal reservoir model with spheroids of anisotropy ratio $e = 1:1$ (circles), $e = 2:1$ (triangles), $e = 5:1$ (diamonds), $e = 10:1$ (plusses), $e = 15:1$ (crosses) and $e = 30:1$ (squares). The analytical curves are obtained from the generalized self-consistent relations for a composite of aligned oblate spheroids, equation (2.8) in the text.

generalized self-consistent relations (*cf.* symmetric versus asymmetric effective medium results for spheres). The percolation effect is most significant for small anisotropy ratios and tends to lower the effective permeability data relative to the analytical curves. Although it is true that the analytical curves do not achieve a percolation threshold for any value of e, they approximate percolation behaviour for $e \geq 10$.

(ii) Allowing overlapping effectively increases the correlation length of the shales, tending to increase the values of the simulation data relative to the analytical curves. This effect is most prominent at large anisotropy ratios.

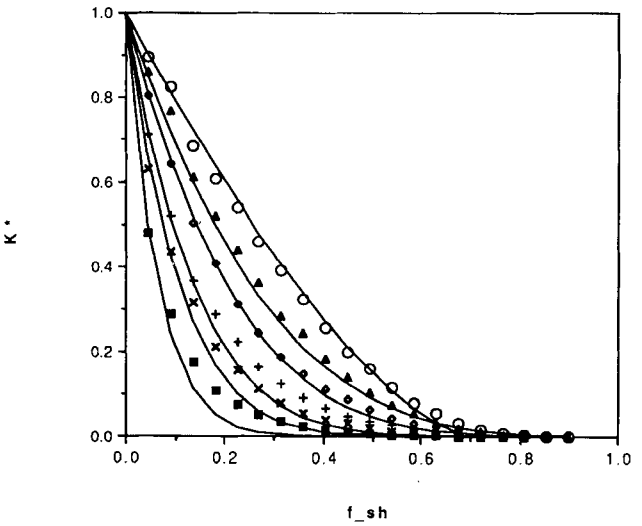

Figure 9. The data are as in Fig. 8. The solid curves are the generalized percolation model fits to the data.

Table 1. Values of the parameter m [see equation (2.18) in the text] which were fitted to the numerical effective permeability curves computed in simulations of the spheroidal reservoir model with spheroidal inclusions of varying anisotropy ratio, e, and for two different values of the permeability contrast ratio, α.

	$e = x : z$	m
$\alpha = 0.0001$	1:1	0.4
	2:1	0.30
	5:1	0.23
	101	0.14
	15:1	0.11
	30:1	0.07
	3:3	0.56
	6:3	0.45
	15:3	0.37
	30:3	0.25
$\alpha = 0.1$	2:1	-0.1
	5:1	-0.3
	10:1	-0.5
	15:1	-0.6
	30:1	-0.8

Fig. 9 shows the curves which have been fitted to the simulation data of Fig. 8 using the generalized percolation model. Table 1 gives the values of the parameters m and f_c (see equation 2.18) fitted to the data for various values of the anisotropy ratio, e. Except for $e = 1:1$, it was found that it was acceptable to set $f_c = 1$, and to use a one-parameter fit for the exponent m, corresponding to the power-averaging method. When $e = 1:1$ percolation theory is known to apply and gives the percolation threshold to be $f_c = 0.6883 \pm 0.0005$. Even in this case, however, power-averaging gives an acceptable fit to the computed data for $f_{sh} < 0.5$. Anyway, this is an artificial geometry. In practical cases it is expected that it will always be acceptable to set $f_c = 1$ (no percolation threshold behaviour) and to use a one-parameter fit as required by the power-averaging method. For $e \geq 10$ it is no longer possible to choose one value of m to fit both the dilute (low f_{sh}) and concentrated (high f_{sh}) effective permeability data as the analytical power-averaging curve has the wrong shape. We have chosen to fit the dilute results in Fig. 9.

Fig. 10 shows the results of geostatistical simulations compared with the previous data from the spheroidal model (Fig. 8). The geostatistical results are in close agreement with the spheroidal results for the entire range of anisotropy ratios simulated, which is remarkable considering that the permeability realizations were generated in completely different ways in the two models. The geostatistical realizations were generated using quite sophisticated

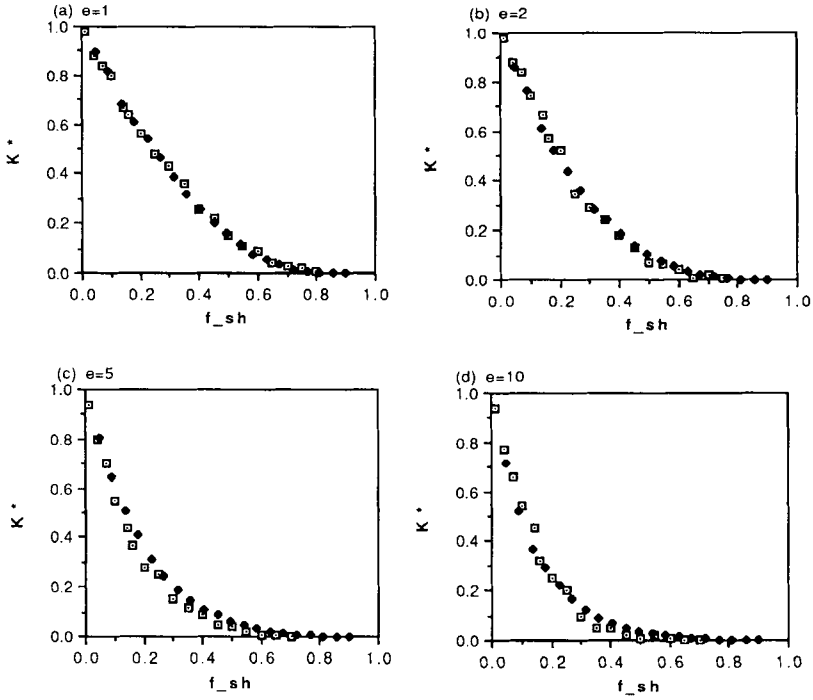

Figure 10. Effective permeability data computed in simulations of the geostatistical model (squares) and the spheroidal model (diamonds): (a) $e = 1:1$, (b) $e = 2:1$, (c) $e = 5:1$ and (d) $e = 10:1$.

techniques modelling the first- and second-order moments of a real sand–shale outcrop. They have shales of varying dimensions, resulting from a specified exponential fall-off of correlations. The spheroidal realizations contain shale inclusions of constant dimensions and can only mimic the statistical characteristics of a real sand–shale geometry through the randomizing effects of overlapping and periodicity (see Fig. 5). The similarity of the results for the two models is reassuring in the sense that it means that one can use relatively simple models, such as overlapping spheroids of a constant dimensions, to reproduce the main features of the effective permeability curve of an inherently much more complex sand–shale geometry. Factors such as the exact form of the shale correlations are not important relative to factors such as the degree of anisotropy.

Figs 11 and 12 show the results of randomly orienting a

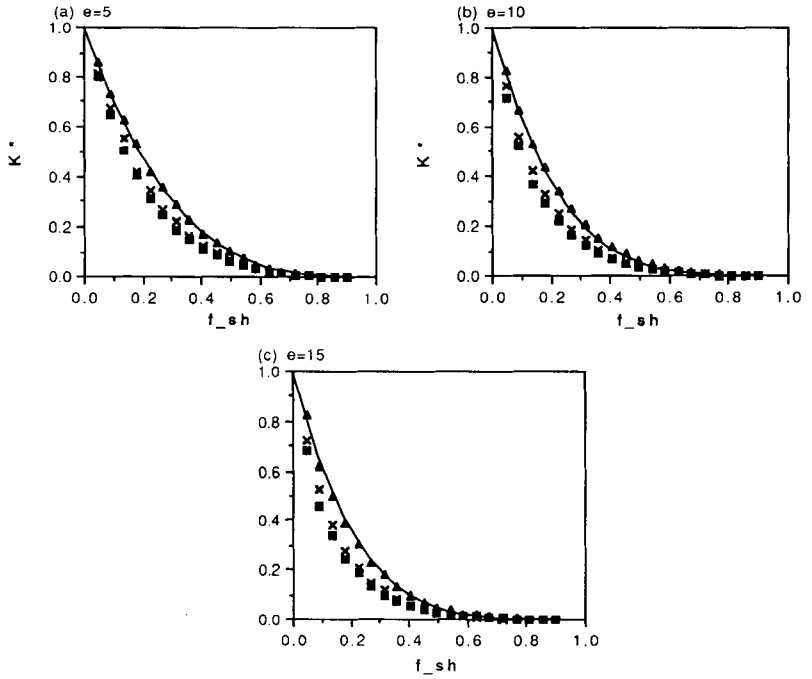

Figure 11. Effective permeability data computed in the simulations of the spheroidal reservoir model with completely aligned spheroidal inclusions (squares), half randomly oriented (crosses), and completely randomly oriented (triangles): (a) $e = 5:1$, (b) $e = 10:1$ and (c) $e = 15:1$. The solid curves are the generalized percolation model fits to the data for completely randomly oriented spheroids.

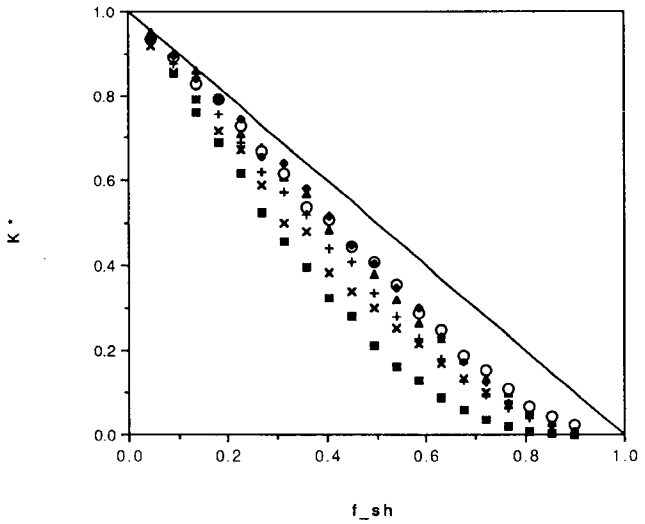

Figure 12. (a), (b) and (c) show the effective horizontal permeability data corresponding to the simulations described for Fig. 11. (d) shows the effective horizontal permeability data computed in simulations with spheroids of anisotropy ratio $e = 1:1$ (squares), $e = 2:1$ (crosses), $e = 5:1$ (plusses), $e = 10:1$ (triangles), $e = 15:1$ (diamonds) and $e = 30:1$ (circles). The solid curve is the arithmetic mean.

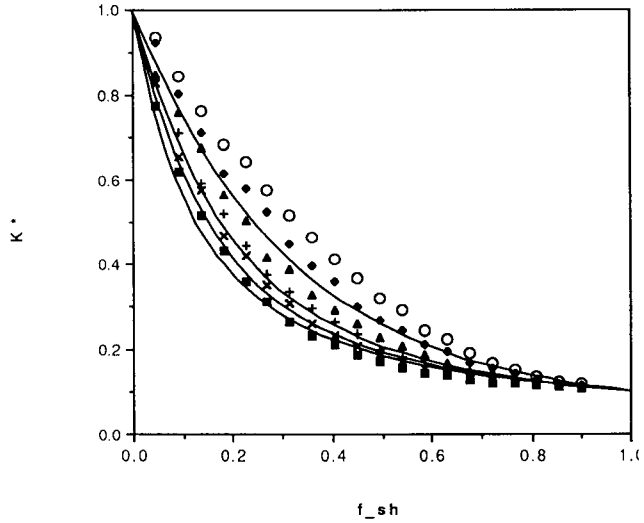

Figure 13. Effective permeability data computed in simulations of the spheroidal reservoir model with a value of the permeability contrast ratio of $\alpha = 0.1$ and with spheroids of anisotropy ratio $e = 1:1$ (circles), $e = 2:1$ (diamonds), $e = 5:1$ (triangles), $e = 10:1$ (plusses), $e = 15:1$ (crosses) and $e = 30:1$ (squares). The solid curves are obtained from the generalized self-consistent relation for aligned oblate spheroids, equation (2.8) in the text.

certain percentage of the aligned spheroidal inclusions. As intuitively expected, the effect of randomizing their orientation is to increase the effective vertical permeability and decrease the effective horizontal permeability. This effect becomes more important as the anisotropy ratio is increased. The results of simulations in which all of the spheroidal inclusions were randomly oriented are well-fitted by a power-averaging curve, as shown in Fig. 11.

Fig. 12(d) shows the effective horizontal permeability calculated in simulations of the aligned spheroidal reservoir model. As the anisotropy ratio increases, the effective horizontal permeability tends towards the arithmetic mean, which is the exact result for a medium with aligned cylindrical inclusions. Hence; for strongly anisotropic media it is reasonable to use the arithmetic mean as an estimate of the effective horizontal permeability. However, it has been demonstrated in this paper that it is not possible to use the (corresponding) harmonic mean estimate for the effective vertical permeability when the permeability contrast ratio is close to zero. It is clearly the case that even small horizontal variations significantly enhance vertical flow.

4.4 Results for $K_{sh}/K_{ss} \equiv \alpha = 0.1$

Fig. 13 shows the results obtained for the effective permeability of the spheroidal reservoir model when the permeability contrast ratio, α, was set to $\alpha = 0.1$. The analytical curves shown in the figure are those derived from the generalized self-consistent scheme for aligned oblate spheroids, equation (2.8). The self-consistent curves provide an acceptable fit to the data for anisotropy ratios $e \geq 5$. Alternatively, a one-parameter, power-averaging fit to the data can be made. The values which were found for the fitted parameter, m, are given in Table 1. Note that for strongly anisotropic systems the effective permeability curve approaches the harmonic mean, corresponding to $m = -1$.

5 CONCLUSIONS

The numerical data generated in the simulations described in this paper have been used to estimate upper and lower bounds for the effective vertical permeability curve of a sand–shale reservoir with a given anisotropy ratio, e, and with a permeability contrast ratio, $\alpha \leq 0.01$. The bounds are in the form of the generalized percolation model, equation (2.18), and the corresponding values of the exponent m for different values of e are shown in Table 2. Also shown are the exponents predicted by dilute suspension theory for aligned spheroidal inclusions, $m_{\text{dilute}} = 1 - L$ (see Section 2.2). It is expected that effective permeability data will lie between the bounds specified in Table 2 and that the following relative statements about their dependence on geometrical factors will hold:

(i) greater variance in the length of the shale inclusions will lead to higher effective permeability values;

Table 2. Values of the exponent m [see equation (2.18) in the text] which give empirical lower, m_{low}, and upper, m_{up}, bounds for the effective permeability data generated in the simulations described in this paper for different values of the anisotropy ratio, e. The exponent m_{dilute} is predicted from the dilute suspension theory (see Section 2.1 in the text).

e	m_{low}	m_{up}	m_{dilute}
1	0.33	0.67	0.67
2	0.33	0.50	0.48
5	0.22	0.40	0.25
10	0.14	0.25	0.14
15	0.10	0.20	0.10
30	0.05	0.13	0.05

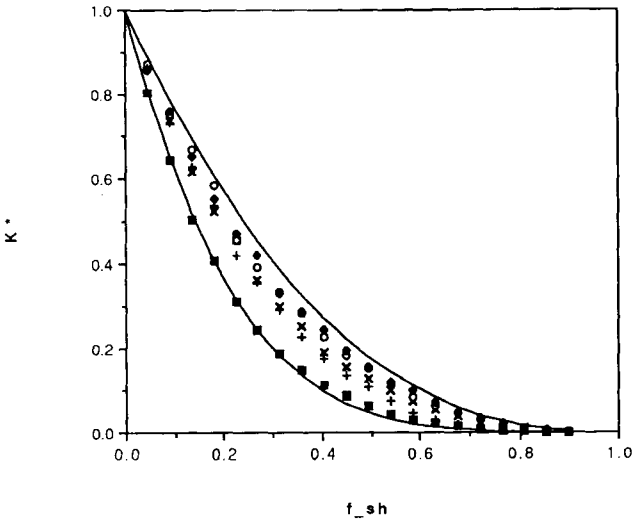

Figure 14. Effective permeability data computed in simulations of the spheroidal reservoir model with spheroids of anisotropy ratio $e = 5:1$ (squares), $e = 10:2$ (crosses), $e = 15:3$ (diamonds), $e = 20:4$ (circles) and completely randomly oriented spheroids of anisotropy ratio $e = 5:1$ (plusses). The solid curves are the suggested empirical bounds.

(ii) greater randomness in the orientation of the shale inclusions will lead to higher effective permeability values; and

(iii) a symmetric-type geometry with a percolation effect will lead to lower effective permeability values.

Fig. 14 shows the empirical bounds of Table 2 together with all the effective permeability data computed in simulations of reservoir models with an anisotropy ratio of $e = 5$.

In this paper a study has been made of the dependence of the effective permeability of sand–shale reservoirs on the geometry of the shale inclusions. Numerical simulations have been described in which factors such as the orientation and the degree of anisotropy of the shales, their volume fraction and the permeability contrast ratio between the shale and the sandstone were varied. Two different reservoir models were used in the simulations: one in which the shales were in the form of random, overlapping spheroidal inclusions, and one in which the shales were generated by a geostatistical technique. The numerical data have been compared with a variety of analytical models. As a result of the study, it has been possible to give empirical bounds for the vertical effective permeability curve of a sand–shale reservoir with a given anisotropy ratio, and to make inferences about the influence of various geometrical factors on where actual effective permeability data values will lie within those bounds.

ACKNOWLEDGMENTS

I would like to thank Professor I. Lerche (Department of Geological Sciences, University of South Carolina) and Dr A. A. Inayat-Hussain for helpful discussions and The Broken Hill Proprietary Co. Ltd for permission to publish this paper.

REFERENCES

Aziz, K. & Settari, A., 1979. *Petroleum Reservoir Simulation*, Applied Science Publishers, London.

Batchelor, G. K., 1974. Transport properties of two-phase materials with random structure, *Ann. Rev. Fluid Mech.*, **6**, 227–255.

Begg, S. H. & King, P. R., 1985. Modelling the effects of shales on reservoir performance: Calculation of effective vertical permeability, *Paper SPE 13529*, presented at the SPE Reservoir Simulation Symposium, Dallas, February 10–13.

Begg, S. H., Chang, D. M. & Haldorsen, H. H., 1985. A simple statistical method for calculating the effective vertical permeability of a reservoir containing discontinuous shales, *Paper SPE 14271* presented at the 60th Annual Technical Conference and Exhibition of the SPE, Las Vegas, September 22–25.

Begg, S. H., Carter, R. R. & Dranfield, P., 1989. Assigning effective values to simulator gridblock parameters for heterogeneous reservoirs, *SPE Res. Eng.*, November, 455–463.

Benveniste, Y. & Miloh, T., 1989. An exact solution for the effective thermal conductivity of cracked bodies with oriented elliptical cracks, *J. appl. Phys.*, **66**, 176–180.

Bergman, D. J., 1982. Rigorous bounds for the complex dielectric constant of a two-component composite, *Ann. Phys.*, **138**, 78–114.

Böttcher, C. J. F., 1945. The Dielectric constant of crystalline powders, *Rec. Trav. Chim. Pays-Bas*, **64**, 47–51.

Coniglio, A., 1975. Some cluster-size and percolation problems for interacting spins, *Phys. Rev.*, B, **13**, 2194–2207.

Dagan, G., 1979. Models of groundwater flow in statistically homogeneous porous formations, *Water Resources Res.*, **15**, 47–63.

Desbarats, A. J., 1987a. Stochastic modeling of flow in sand–shale sequences, *PhD thesis*, Department of Applied Earth Sciences, Stanford.

Desbarats, A. J., 1987b. Numerical estimation of effective permeability in sand–shale formations, *Water Resources Res.*, **23**, 273–286.

Deutsch, C. V., 1989. Calculating effective absolute permeability in sandstone/shale sequences, *SPE Form. Eval.*, September, 343–348.

Drummond, I. T. & Horgan, R. R., 1987. The effective permeability of a random medium, *J. Phys., A: Math. Gen.*, **20**, 4661–4672.

Dupuy, M. & Lefebvre du Prey, E., 1968. L'anisotropie d'ecoulement en milieu poreux presentant des intercalations horizontales discontinues, *3ieme Colloque de la ARTFP*, Pau, September 23–26.

Evans, J. W., 1987. Correlated percolation: exact Bethe lattice analyses, *J. Phys., A: Math. Gen.*, **20**, 6487–6500.

Haldorsen, H. H., 1989. On the modeling of vertical permeability barriers in single-well simulation models, *SPE Form. Eval.*, September, 349–358.

Hale, D. K., 1976. The physical properties of composite materials, *J. Mat. Sci.*, **11**, 2105–2141.

Hashin, Z. & Shtrikman, S., 1962. A variational approach to the theory of the effective magnetic permeability of multiphase materials, *J. appl. Phys.*, **33**, 3125–3131.

Haus, J. W. & Kehr, K. W., 1987. Diffusion in regular and disordered lattices, *Phys. Rep.*, **150**, 263–406.

Havlin, S. & Ben-Avraham, D., 1989. Diffusion in disordered media, *Adv. Phys.*, **36**, 695–798.

Journel, A. G., Deutsch, C. V. & Desbarats, A. J., 1986. Power averaging for block effective permeability, *Paper SPE 15128*, presented at the 1986 SPE California Regional Meeting, Oakland, April 2–4.

Kikuchi, R., 1970. Concept of the long-range order in percolation problems, *J. Chem. Phys.*, **53**, 2713–2718.

King, P. R., 1987. The use of field theoretic methods for the study of flow in a heterogeneous porous medium, *J. Phys., A: Math. Gen.*, **20,** 3935–3947.

Kirkpatrick, S., 1973. Percolation and conduction, *Rev. Mod. Phys.*, **45,** 574–588.

Maxwell, J. C., 1873. *Electricity and Magnetism*, 1st edn, p. 365, Clarendon Press, Oxford.

McCarthy, J. F., 1990a. Effective permeability of sandstone–shale reservoirs by a random walk method, *J. Phys., A: Math. Gen.*, **23,** L445–L451.

McCarthy, J. F., 1990b. Effective conductivity of many-component composites by a random walk method, *J. Phys., A: Math. Gen.*, **23,** L749–L753.

McLachlan, D. S., 1987. An equation for the conductivity of binary mixtures with anisotropic grain structures, *J. Phys., C: Solid State Phys.*, **20,** 865–877.

Milton, G. W., 1987. Multicomponent composites, electrical networks and new types of continued fractions 1, 2, *Comm. Math. Phys.*, **111,** 281–327, 329–372.

Milton, G. W. & Kohn, R. V., 1988. Variational bounds on the effective moduli of anisotropic composites, *J. Mech. Phys. Solids*, **36,** 597–629.

Pike, G. E. & Seager, C. H., 1974. Percolation and conductivity: A computer study, *Phys. Rev.*, B, **10,** 1421–1434.

Polder, D. & Van Santen, J. H., 1946. The effective permeability of mixtures of solids, *Physica*, **12,** 257–271.

Schwartz, L. M. & Banavar, J. R., 1989. Transport properties of disordered continuum systems, *Phys. Rev.*, B, **39,** 11 965–11 969.

Sen, A. K. & Torquato, S., 1989. Effective conductivity of anisotropic two-phase composite media, *Phys. Rev.*, B, **39,** 4504–4515.

Smith, L. & Freeze, R. A., 1979. Stochastic analysis of steady state groundwater flow in a bounded domain 1: One dimensional simulations, *Water Resources Res.*, **15,** 1543–1559.

Stauffer, D., 1985. *Introduction to Percolation Theory*, Taylor & Francis, London.

Wiener, O., 1912. *Abhandl.* Math. Phys. Klasse Sächs, Akad. Wiss. Leipzig, **32,** 509.

Willis, J. R., 1977. Bounds and self-consistent estimates for the overall properties of anisotropic composites, *J. Mech. Phys. Solids*, **25,** 185–202.